CFD-Stall Untersuchung des Neues Tragflächenprofil für HAWT im Vergleich zu messtechnische von Windkanalversuchs

CFD stall investigation of novel airfoil design for HAWT compared with measurements of wind tunnel experiment

Youjin Kim[1,2], Ali Al-Abadi[3], Antonio Delgado[1,2]
[1]Institute of Fluid Mechanics, FAU Busan Campus, University of Erlangen-Nuremberg, Republic of Korea
[2]Institute of Fluid Mechanics, University of Erlangen-Nuremberg, Germany
[3]SGB Power Transformers, R & D Department, Regensburg, Germany

Keywords: CFD, Wind Tunnel, Airfoil, Aerodynamics, Renewable Energy

Abstract

The stall of the airfoil S809 used in Horizontal Axis Wind Turbine (HAWT) of NREL UAE Phase VI has been investigated via CFD simulation of software OpenFoam® with implementation of the Spalart-Allmaras turbulence model and Gmsh meshing method. Result are compared with the experimental descriptions of airfoil S809. The resultant coherent stall characterization is used to proceed further on optimization of the airfoil. The optimized airfoil, named S809gx, is made based on airfoil S809 to upgrade its GR (Gliding Ratio) and Xtr (transition points) for higher aerodynamic efficiency and enlarged laminar boundary layer of the airfoil. The drag coefficient, boundary layer thickness, and skin-friction coefficient of the airfoil with controlled boundary layer are calculated by XFOIL. The comparison between the reference airfoil S809 and the optimized airfoil S809gx proves the advantageous of the surface shape of preliminarily designed airfoil S809gx. The power production simulations of HAWT with two airfoils are done to demonstrate the positive influence of airfoil S809gx on turbine unit.

Introduction

When an airfoil is encountered with the specifically enlarged angle of attack caused by sudden change in wind speed and direction, the stall on airfoil surface occurs. The suction side of the airfoil experiences the adverse pressure gradient to provoke the flow on the upper side to be separated and it causes dropped lift force of the airfoil. The process of stall includes sophisticated aerodynamic flow motions such as turbulence transition, unstable shear layer, vortex phenomena, etc [1].
The unsteady wind inflow, yaw misalignment, tower shadow, rapid wind speed increment, wind gusts are the elements for rapidly changed blade angle of attack to cause the dynamic stall. Because the unsteady loads on the HAWT are mainly caused by dynamic stall, the study of stall dynamic effects on the HAWT blades is necessary [2].
The Laminar Separation Bubble (LSB) is formed when the laminar flow is separated by the adverse pressure gradient and reattached. The circulatory flow motion is formed to be called

as the bubble with reverse flow vortex inside of it. The bubbles affect aerodynamic of flow over the airfoil in an undesirable way, especially the bubble formation generates an increasing drag and change in pitching moment. If the large bubble is formed and the shear layer is not reattached, then the lift efficiency is drastically decreased [3]. Therefore, the airfoil shape with smaller LSB number is desirable.

In this study, the stall of airfoil S809 of NREL Phase VI is investigated by CFD with the comparison of its experimental results. The same CFD is used for simulating newly designed airfoil S809gx. The results are compared with the reference airfoil S809 for laminar separation bubbles occurrence and stall formation. The results convinced its upgraded efficiency compared to the reference airfoil.

Airfoil Stall CFD calculation

OpenFoam® with Spalart-Allmaras turbulence model and Gmsh meshing are used in the current simulation. The Gmsh tool offers a certain tool for mesh refinement so that the validity of the mesh results can be assured of its reliability. As the 6 decimals of accuracy are used, the changes are only appreciated by the 4th digit with the maximum of 0.1%, [4], Figure 1.
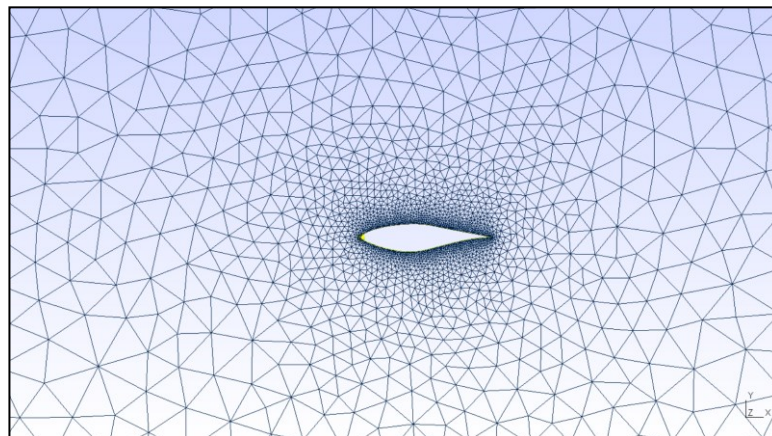

Figure. 1: The mesh for airfoil S809 by Gmsh

The airfoil stall investigation can be categorized as the incompressible flows with the requirement of turbulence modeling, the solver is chosen as SimpleFoam. The turbulence model, Spallart-Allmaras model for RANS is chosen because the OpenFoam® allows the user to skip coding or editing on the model as those are already built in software. The Para-View® was used for post-processing of the result [5].

CFD and Experimental results comparison

The flow visualizations for airfoil S809 were done for the angle of attacks 4, 6.75 and 21.95 degrees, which were the values for fully attached, transition-separation and dynamic stall regimes, respectively.

The simulation results show the turbulent, trailing edge separation occurrence on the suction side of the airfoil and the separated flow. Further, the stall phenomena is apparent as the angle of attack increases, which is the coherent founding with the experimental results.

While the experiment result showed the detailed laminar separation bubble in lower angle of attack, CFD results couldn't illustrate it. However, the CFD results present the detailed chro-

nology of separation, stall and laminar separation bubbles formation and propagation processes. The bubbles are observed to be moving toward downstream when an angle of attack increases with constant bubble length in the experiment. The bubbles movement tendency are found to be the same from both experiments and CFD simulations. The experiments have different angle of attack to move the bubble formation location, whereas CFD results show same movement at constant stall regime angle of attack with simulation time variation [6], figure 2.
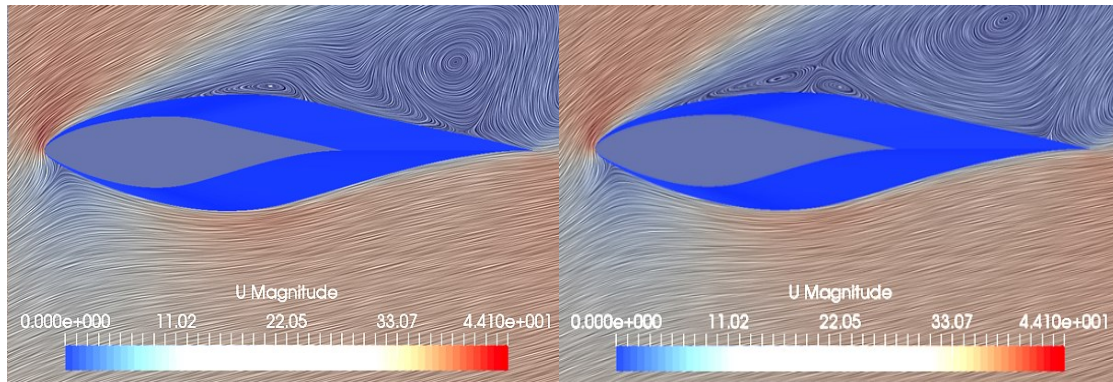
Figure. 2: CFD simulation for S809 to compare LSB formation

Optimized Airfoil

The optimized airfoil, named S809gx, is made based on airfoil S809 to upgrade its GR (Gliding Ratio) and Xtr (transition points) for higher aerodynamic efficiency and enlarged laminar boundary layer. Figure 3. The B-Spline parameterization of the airfoil and its optimization are programmed in MATLAB® for generating the optimization process of the airfoil. The GA optimization process is interfaced by airfoil flow solver XFOIL, which is based on the linear-vorticity panel method, e^9-type amplification formulation, and transonic ISES code [7].

The transition point in the boundary layer and the GR value of airfoil are selected to be maximized in multi-objective function in GA optimization algorithm. In addition, the laminar boundary layer region of airfoil is aimed to be enlarged for the advantageous airfoil shape in terms of reducing turbulent generation at the surface of the airfoil. The increased GR values of S809 for each flow regime (for Fully Attached FA, Transition Tr and Stall for dynamic stall regime) are calculated at different angle of attacks. The values indicate the optimized airfoil have the increased aerodynamic efficiency, figure 4.
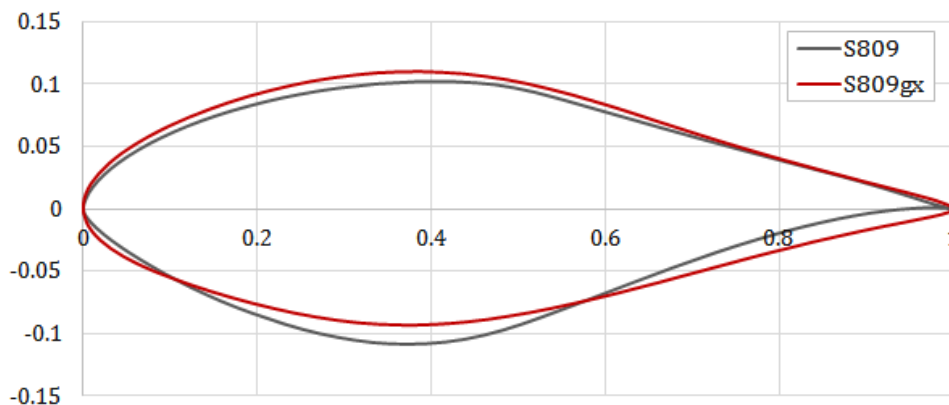

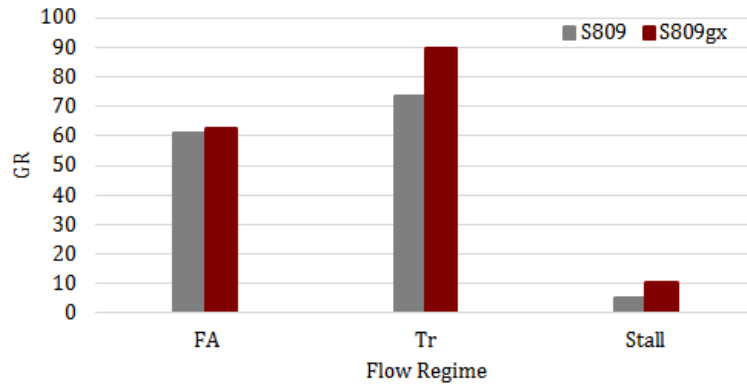Figure. 3: Airfoil S809 and optimized airfoil S809gx

Figure. 4: GR comparison for airfoil S809 and S809gx for all flow regimes

The expanded laminar boundary layer region of airfoil caused the friction and pressure drag decrement. The reduced thickness of boundary layer and skin-friction coefficient values explaines the decreased drag values of the airfoils. The comparisons of boundary layer thickness and skin-friction coefficient of the upper surface of the airfoil S809 and S809gx are shown in figure 5.
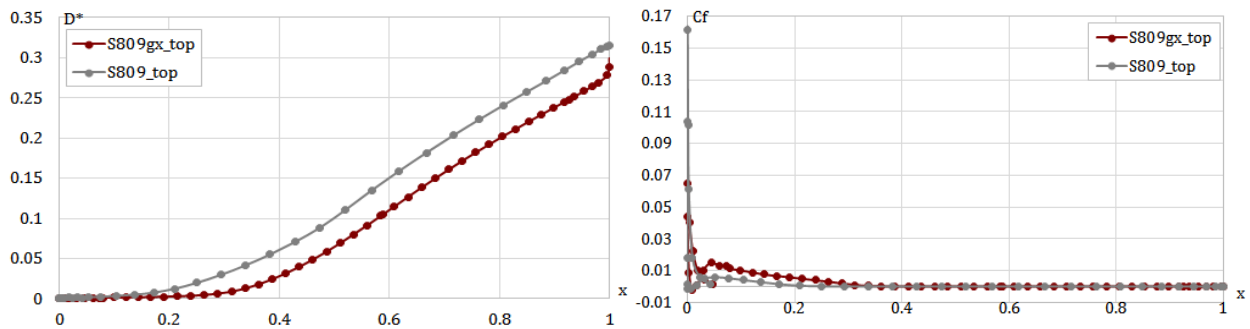

Figure. 5: Boundary layer thickness and skin-friction coefficient of the airfoils

CFD results comparison

The simulation results of airfoil S809 and S809gx are compared for observing their LSB formation and chronology of stall propagation. The airfoil S809gx has 50% smaller laminar bubble formation number during the simulation time T=1000 with time interval T=50.
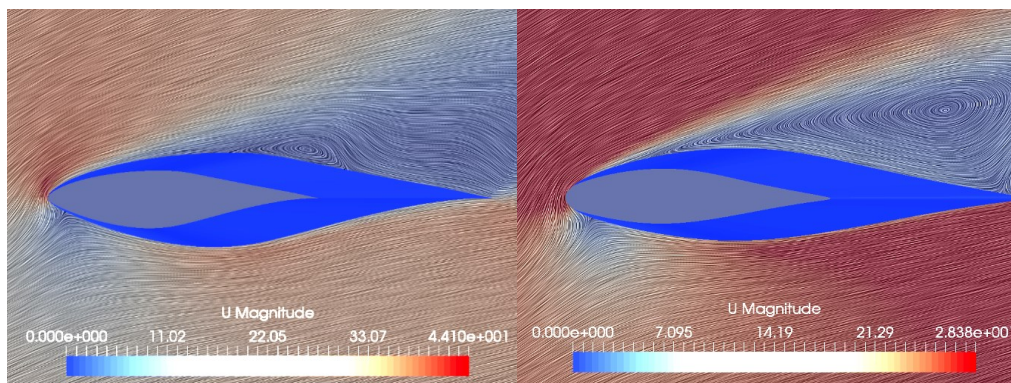

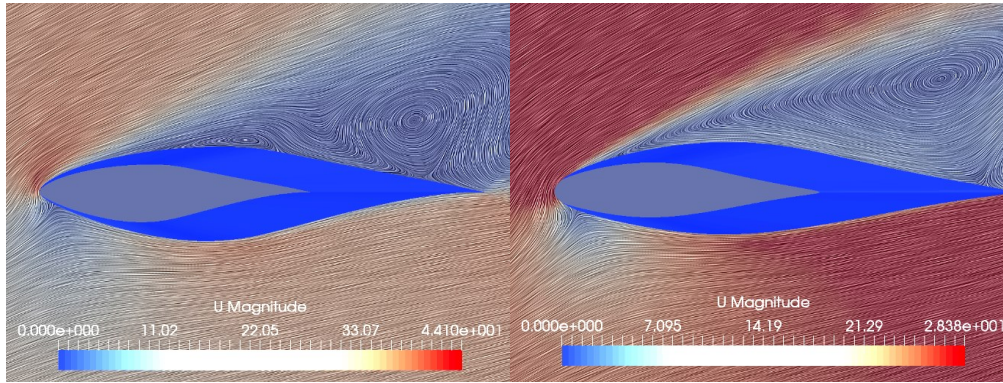Figure. 6: CFD results comparison for S809 and S809gx at T=250

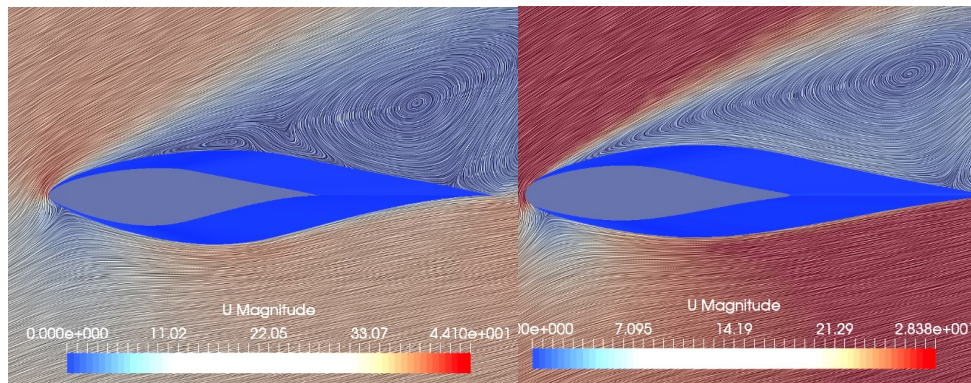Figure. 7: CFD results comparison for S809 and S809gx at T=450

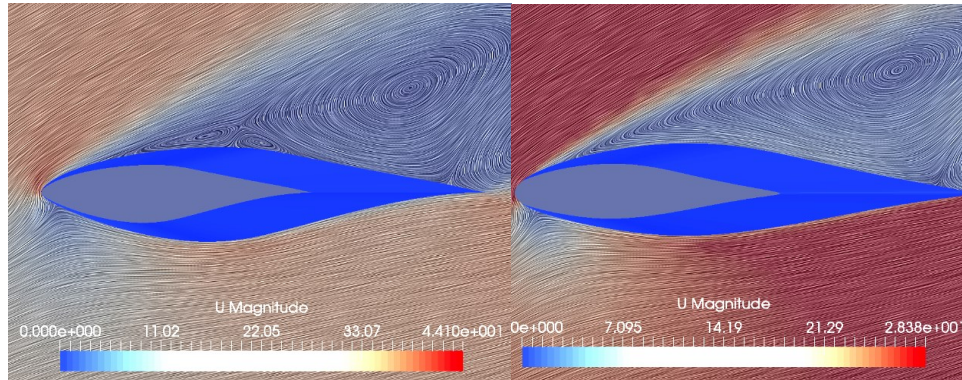Figure. 8: CFD results comparison for S809 and S809gx at T=650

Figure. 9: CFD results comparison for S809 and S809gx at T=850

In Figure 6 – 9, the airfoil S809 show LSB formation on the upper surface at T=250, 450, 650, 850. Especially at T=850, two LSBs are found on the airfoil S809 whereas no LSB is found in the airfoil S809. As the airfoil S809gx has less number of LSB generation, it can be exempted from the undesirable effect of LSB compared to the airfoil S809. For example, the airfoil S809gx can be free from the increased drag and pitching moment change caused by LSB, which are undesirable aerodynamic inefficiency for HAWT blade performance.

HAWT Power production comparison

The power production calculations for two HAWR blades with different airfoils, S809 and S809gx are done with software Qblade. The blades are designed to have the same blade design characteristics of NREL Phase VI [6], with only changing airfoil shapes.

	NREL Phase VI with airfoil S809	NREL Phase VI with airfoil S809gx
Power Regulation	Stall	Stall
Transmission	Single	Single
V cut in/ cut out [m/s]	6 / 25	6 / 25
Rotational Speed [rpm]	71.63	71.63
Outer Radius [mm]	5532	5532
Variable Losses	0.22	0.22
Fixed Pitch/ Fixed Loss	0	0
Weibull Setting	k 2($\pm$3) A 9($\pm$3)	k 2($\pm$3) A 9($\pm$3)
Annual Yield [W]	49461730	59404491

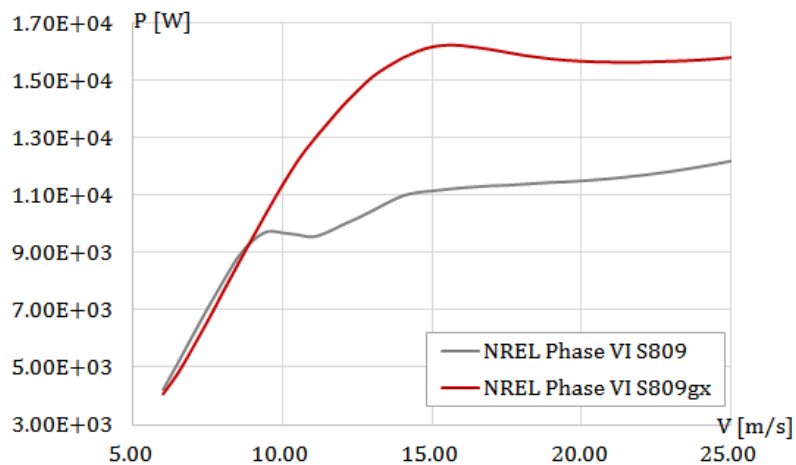Table. 1: The settings for simulation of HAWT performance for two different airfoils

Figure. 10: Power-velocity curves for turbines

The HAWT with the blade of S809gx shows higher power production from the velocity point ≈8 m/s, whereas power difference below the point is negligible. The airfoil S809gx with increased GR and smaller LSB formation at stall flow regime affects the power production of HAWT to have the desirable increment.

Conclusion

The CFD simulation for visualization the HAWT airfoil S809 for stall phenomena is performed. Comparison of the CFD with the experimental results shows the coherent context of stall occurrence. The turbulent and trailing edge separation are occurred on the suction side of the airfoil. The separated flow with stall phenomena is apparent as the angle of attack increased. The LSBs are observed to be moved toward downstream when the angle of attack increase with constant bubble length in the experiment. The same bubble movement behavior is found from the CFD result.

The upgraded airfoil S809gx, which is optimized from S809, is aimed to improve GR and Xtr for higher aerodynamic efficiency and enlarged laminar boundary layer. The increased GR values of S809 for different flow regime of range of angle of attacks are calculated. It shows that the optimized airfoil has higher aerodynamic efficiency. The boundary layer thickness and skin-friction coefficient value of the airfoil S809gx are shown to prove a lower friction and pressure drag.

The CFD comparison of the airfoils of S809 and S809gx shows that occurrence number of LSB was smaller at S809gx. It shows that S809gx has the advantageous surface shape to avoid adverse pressure gradient causing LSB in the same dynamic stall angle of attack condition. The power production simulation shows the aerodynamic advantages of optimized airfoil S809gx that led to improved performance of HAWT.

Acknowledgement

Literature

[1] K. Mulleners, A. L. Pape, 2012: The Dynamics of Static Stall, 16th Int Symp on Applications of Laser Techniques to Fluid Mechanics, Lisbon, Portugal

[2] A. Choudhry, M. Arjomandi, R. Kelso, 2012 :Estimation of Dynamic Stall on Wind Turbine Blades using an Analytical Model, 18th Australasian Fluid Mechanics Conference, Launceston, Australia

[3] Mohsen Jahanmiri, 2011: Laminar Separation Bubble: Its Structure, Dynamics and Control, CHALMERS UNIVERSITY OF TECHNOLOGY, Sweden, Research report 2011:06

[4] S.J.R.Sánchez, 2014: Analysis of flow separation over aerodynamic airfoils, Bachelor thesis, Aerospace Engineering, UNIVERSIDAD CARLOS III DE MADRID ESCUELA POLITÉCNICA SUPERIOR

[5] S.Deck, P.Duveau,P.d'Espiney, P.Guillen, 2002: Development and application of Spalart-Allmaras one equation turbulence model to three-dimensional supersonic complex configurations, Aerospace Science and Technology 6, pp. 171–183, Elsevier

[6] Dan M. Somers: Design and Experimental Results for the S809 Airfoil, Dan M. Somers, NREL/SR-440-6918

[7] Mark Drela: XFOIL: An Analysis and Design System for Low Reynolds Number Airfoils, MIT dept. of Aeronautics and Astronautics, Cambridge, Massachusetts